CrystEngComm

Enantiopure and quasiracemic crystals of 7-substituted tryptophan derivatives: modulation of molecular arrangement for functionalized crystals

Journal:	*CrystEngComm*
Manuscript ID	CE-ART-01-2025-000099.R2
Article Type:	Paper
Date Submitted by the Author:	28-Mar-2025

Complete List of Authors:	Tsuchiya, Yuiho; Yokohama National University, Department of Chemistry and Life Science, Graduate School of Engineering Science Ohata, Misaki; University of Shizuoka, School of Food and Nutritional Sciences Chisuga, Taichi; University of Shizuoka, School of Food and Nutritional Sciences Nakano, Shogo; University of Shizuoka, School of Food and Nutritional Sciences; Japan Science and Technology Agency, PRESTO Ito, Suguru; Yokohama National University, Department of Chemistry and Life Science, Graduate School of Engineering Science; Japan Science and Technology Agency, PRESTO

ARTICLE

Enantiopure and quasiracemic crystals of 7-substituted tryptophan derivatives: modulation of molecular arrangement for functionalized crystals

Received 00th January 20xx,
Accepted 00th January 20xx

DOI: 10.1039/x0xx00000x

Yuiho Tsuchiya,[a] Misaki Ohata,[b] Taichi Chisuga,[b] Shogo Nakano[bc] and Suguru Ito*[ac]

Amino acids are widely distributed in natural systems, and their crystals hold great promise as functional materials. However, the variety of natural amino acid is inherently limited. In this study, the crystal structures and properties of two 7-substituted tryptophan derivatives have been investigated. The crystal of L-7-cyanotryptophan exhibited a different molecular arrangement from that of natural L-tryptophan, primarily due to the involvement of the cyano and indole amino groups in forming intermolecular hydrogen bonds. Meanwhile, L-7-azatryptophan formed two distinct crystals, *α* and *β*. In particular, the *α*-crystal featured one-dimensional pores capable of including solvent molecules. Furthermore, co-crystallization of L-7-cyanotryptophan with D-tryptophan afforded a quasiracemic crystal, which exhibited fluorescence at longer wavelength compared with racemic tryptophan crystal.

Introduction

Amino acids are abundant in nature and play important biological roles as the components of proteins.[1,2] The crystal structures of all 20 proteinogenic amino acids have been determined, and polymorphs have been reported for 11 of them.[3] Amino acid crystals are attractive due to their diverse advantages, including low cost, ease of production, inherent biocompatibility, and biodegradability. These features have driven recent investigations into the applications of amino acid crystals as functional materials with piezoelectric, mechanical, and optical properties.[4] Understanding crystal structures and controlling polymorphs[5] would further advance the development of functional amino acid crystals. Moreover, because the variety of natural amino acids is limited, the introduction of substituents or co-crystallization with other molecules can enhance the development of practical and versatile functional amino acid materials.

Preparations of racemic crystals[6] and quasiracemic crystals[7] are valuable methods to regulate the properties of crystals obtained from enantiopure molecules. Compared with enantiopure crystals, racemic crystals are typically formed preferentially due to their densely packed structures and exhibit different physical and functional properties. Furthermore, by taking advantage of the tendency for both enantiomers to arrange complementarily,[8] quasiracemic crystals can be formed using enantiomers with partially different structures, allowing them to coexist within the same crystal lattice. While examples of adjusting the properties of natural amino acid crystals through the formation of quasiracemic crystals remain limited,[9] this approach shows great potential. Combining natural amino acids with non-natural substituted amino acids as quasiracemates is expected to further expand the structural and functional diversity of amino acid crystals.

The reported crystals of tryptophan (**1**) include three polymorphs of L-**1** and one racemic crystal.[2,10] In all these crystals, a layered structure is formed, where hydrophilic and hydrophobic regions are arranged alternately due to extended hydrogen bonding between the carboxylate group (-COO^-) and the protonated amino group (-NH_3^+). Substituted tryptophan derivatives, with modifications to the indole ring while retaining the amino acid moiety, hold potential for the development of functionalized crystals. However, the synthesis of such substituted tryptophan derivatives is challenging, and only a

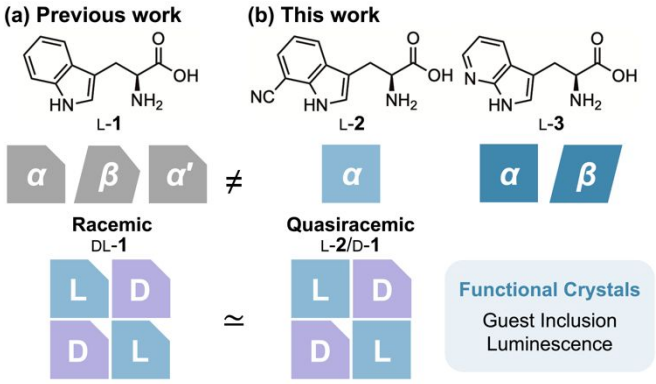

Fig. 1 (a) Previous work: Three polymorphic crystals of L-**1** and racemic crystal DL-**1**. (b) This work: Enantiopure and quasiracemic crystals of L-**2**. Two distinct crystals L-**3**-**α** and L-**3**-**β**.

[a] *Department of Chemistry and Life Science, Graduate School of Engineering Science, Yokohama National University, 79-5 Tokiwadai, Hodogaya-ku, Yokohama 240-8501, Japan. E-mail: suguru-ito@ynu.ac.jp.*
[b] *School of Food and Nutritional Sciences, University of Shizuoka, 52-1 Yada, Suruga-ku, Shizuoka 422-8526, Japan.*
[c] *PRESTO, Japan Science and Technology Agency (JST), 4-1-8 Honcho, Kawaguchi, Saitama 332-0012, Japan.*

† Supplementary Information available: Crystal structures, Hirshfeld surface analysis, BFDH morphology, and theoretical calculations. See DOI: 10.1039/x0xx00000x

limited number of their crystal structures have been characterized.[11]

Herein, crystals of two 7-substituted tryptophan derivatives, L-7-cyanotryptophan (L-**2**) and L-7-azatryptophan (L-**3**), were prepared (Fig. 1). L-**2** and L-**3** were synthesized enzymatically using an engineered L-tryptophan synthase *β*-subunit. The enantiopure crystals of L-**2** and L-**3** differ from the crystals of L-**1** in their arrangement due to the formation of hydrogen bonds involving the 7-cyano and 7-aza groups with adjacent molecules. In particular, L-**3** crystallized into two distinct forms: the *α*-crystal, which includes solvent molecules, and the *β*-crystal, which does not. Furthermore, when L-**2** was co-crystallized with D-**1**, quasiracemic crystals were obtained, exhibiting the same molecular arrangement as the racemic crystals DL-**1** and showing fluorescence in a longer wavelength region compared with DL-**1**.

Results and discussion

Crystal structure of L-7-cyanotryptophan (L-2)

The crystals of L-**2** were obtained as fibrous crystals by vapor diffusion of acetonitrile into an aqueous solution (Fig. S1†), and the structure of crystal L-**2** was determined using the micro electron diffraction method. The molecular packing structure of crystal L-**2** is different from the three polymorphic crystals of L-**1** (Fig. 2, S2–S6†, and Table S1 and S2†).[2,10] Specifically, the crystal L-**2** (space group: $P2_1$) consisted of two crystallographically independent molecules A and B (Fig. 2a).

Hydrogen bonding patterns of L-**2** were characterized by Etter's graph-set analysis (Table S3 and S4†).[12] In the crystal lattice, molecules A and B form a dimer through hydrogen bonding between the amino cation and the carboxylate, resulting in an $R_2^2(10)$ motif (N1A–H1A$\cdots$O1B and N1B–H1B$\cdots$O1A, Fig. 2a right: yellow). The dimers further associate into ABAB-type tetramers through two $D_1^1(2)$ hydrogen bonds (N1B–H2B$\cdots$O2A, Fig. 2a right: violet). These tetramers are stacked along the *b*-axis through continuous hydrogen bonds that form a $C_1^1(5)$ (N1–H3$\cdots$O2, Fig. 2b: pink) motif and a $C_1^2(4)$ (N1A–H1A$\cdots$O1B and N1A–H1A$\cdots$O2B, Fig. 2b: gray) motif via the amino acid moieties, resulting in columnar structures (Fig. 2b and S7†).

The tetramer is arranged in the *ac* plane with translational symmetry (Fig. 2a top). The indole amino group (N2–H4) and the cyano group (N3) participate in hydrogen bonding between tetramers to link the columns (Fig. S7†). Molecule A forms continuous hydrogen bonds with another molecule A in an adjacent tetramer along the [101] direction, resulting in a $C_1^1(6)$ motif (N2A–H4A$\cdots$N3A, Fig. 2a bottom: green). In addition, adjacent tetramers aligned along the *a*-axis are connected via $C_1^1(8)$ hydrogen bonds formed between the indole amino group of molecule B and the carboxylate group of another molecule B (N2B–H4B$\cdots$O1B, Fig. 2a bottom: blue). Furthermore, two $D_1^1(2)$ hydrogen bonds are also formed between molecules BA and AB, involving the amino cation of molecule A and the cyano group of molecule B (N1A–H2A$\cdots$N3B, Fig. 2a bottom: orange).

The Bravais-Friedel-Donnay-Harker (BFDH) method[13] was used to predict the crystal morphology. The crystal morphology of L-**2**, calculated using the BFDH method, exhibits growth along the *b*-axis, which corresponds to the direction of continuous hydrogen bond formation in the stacked tetramers (Fig. 2c). This result should explain the experimental observation that the crystal L-**2** formed the fibrous morphology.

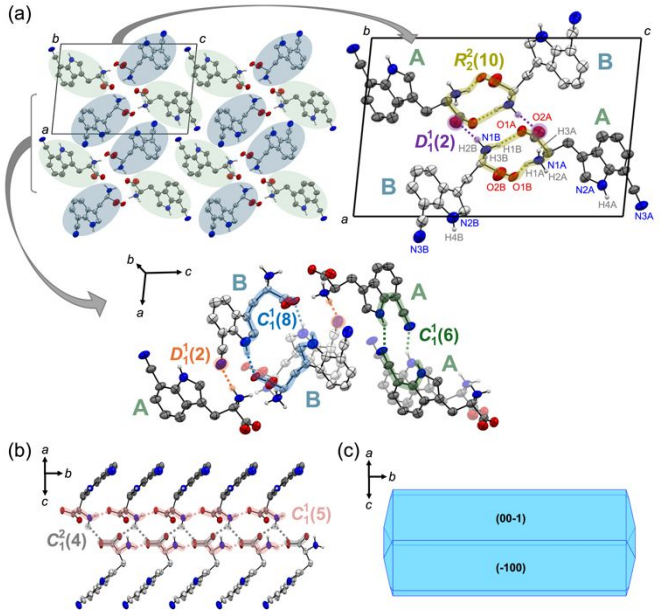

Fig. 2 (a) Packing structures of L-**2**. Dotted lines indicate intermolecular hydrogen bonds. (b) Columnar structure of molecules A and B aligned along the *b*-axis with continuous hydrogen bonds. (c) BFDH morphology of L-**2** predicted from Mercury.[14]

Two crystal structures of L-7-azatryptophan (L-3)

The vapor diffusion of an antisolvent into an aqueous solution of L-**3** afforded two types of crystals, depending on the antisolvent used. When THF was used as the antisolvent, a solvent-including *α*-crystal L-**3-α** was obtained, and single-crystal X-ray structure analysis revealed the presence of one-dimensional pores (space group: *I*4, Fig. 3, S8†, and Table S2†). Although the electron density corresponding to the solvent molecules in the pores was removed using the SQUEEZE method,[15] the ^{1}H NMR spectrum in D_2O confirmed that the *α*-crystal contained L-**3** and THF in a 4:1 molar ratio (Fig. S9†). On the other hand, a solvent-free L-**3-β** (space group: $P2_1$) was obtained when acetonitrile was used as the antisolvent (Table S2†). In both the *α*- and *β*-crystals, the nitrogen atom at the 7-position formed hydrogen bonds with the amino cation, resulting in dimers (Fig. 3a and 3b). These dimers assembled into one-dimensional columns with a two-fold helical axis through continuous hydrogen bonding along the *c*-axis in L-**3-α** and along the *b*-axis in L-**3-β** (Fig. S10†). In L-**3-β**, adjacent columns were related by translational symmetry along the *a*- and *c*-axes (Fig 3b). In contrast, in L-**3-α**, adjacent columns were arranged with a 90° rotational offset, forming one-dimensional pores between four columns that exhibited fourfold rotational symmetry (Fig. 3a). Solvent molecules were included in the pores of L-**3-α**.

To elucidate the differences in the molecular arrangement modes leading to the formation of L-**3-α** and L-**3-β**, the contributions of intermolecular interactions were analyzed using Hirshfeld surface analysis (Fig. S15†). Both the *α*- and *β*-crystals showed a higher contribution of N–H interactions compared to the crystal of L-**1**. However, no significant

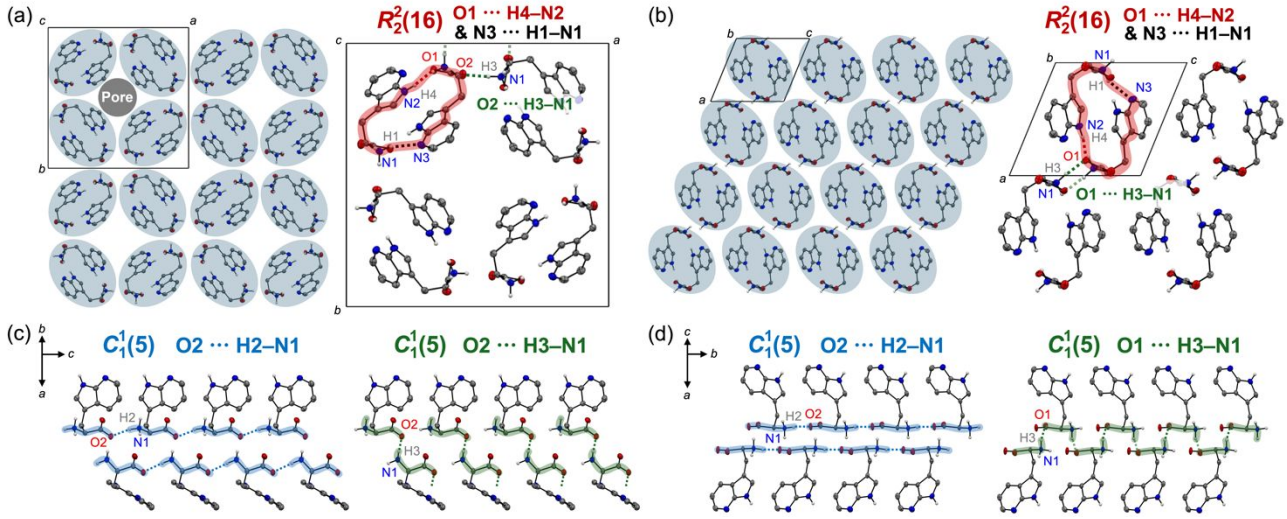

Fig. 3 Molecular arrangements of (a) L-**3-α** viewed along the *c*-axis and (b) L-**3-β** viewed along the *b*-axis. Columnar structures of (c) L-**3-α** and (d) L-**3-β** in the direction of continuous hydrogen bonding. Dotted lines indicate hydrogen bonds between adjacent molecules.

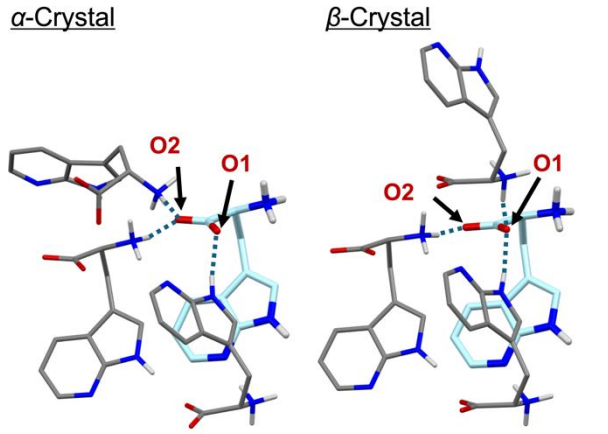

Oxygen atom	Number of hydrogen bonds	
	α-Crystal	*β*-Crystal
O1	1	2
O2	2	1

Fig. 4 Hydrogen bonding interactions of L-**3** in the *α*- and *β*-crystals, where oxygen atoms O1 and O2 form hydrogen bonds with adjacent molecules.

differences were confirmed in the relative contributions of individual interactions between L-**3-α** and L-**3-β**.

The key distinction between L-**3-α** and L-**3-β** is the number of hydrogen bonds formed by the two oxygen atoms, O1 and O2 (Fig. 4). The molecular conformations of L-**3** in the *α*- and *β*-crystals are nearly identical (Fig. S11†). However, in the *α*-crystal, O1 forms one hydrogen bond and O2 forms two, whereas, in the *β*-crystal, O1 forms two hydrogen bonds and O2 forms one. In both crystals, O1 forms a hydrogen bond with the indole amino group (N2–H4) of another molecule, and simultaneously, the nitrogen atom at the 7-position (N3) forms a hydrogen bond with the amino cation (N1–H1), leading to the formation of a cyclic hydrogen-bonded dimer with an $R_2^2(16)$ motif (Fig. 3a and 3b: red, Table S5–S8†). Meanwhile, O2 forms a $C_1^1(5)$ hydrogen bond with the amino cation (N1–H2) along the column extension direction (Fig. 3a and 3b: blue). The remaining O2 in the *α*-crystal and O1 in the *β*-crystal participate in hydrogen bonding with adjacent columns. Although both form $C_1^1(5)$ hydrogen bonds with the amino cation (N1–H3), the hydrogen bonds in the *α*-crystal continuously link four adjacent columns, and those in the *β*-crystal connect two columns in an alternating manner (Fig. 3c, 3d and S8†: green). This difference in the roles of the oxygen atoms in forming hydrogen bonds with adjacent columns can account for the formation of the two distinct crystals, *α* and *β*.

Calculated morphologies obtained by the BFDH analysis indicate that crystal growth in L-**3-α** and L-**3-β** should proceed along the *c*-axis and along the *b*-axis, respectively, corresponding to the direction of column extension formed by hydrogen bonds (Fig. S17†). These observations account for the needle-like morphology of L-**3-α** and the elongated plate-like morphology of L-**3-β** (Fig. S1†).

Quasiracemic crystal of L-**2**/D-**1**

To prepare quasiracemic crystals with different partial structures in the L- and D-forms, L-**2** and L-**3** were individually mixed with D-**1** and crystallized. The combination of L-**2** and D-**1** produced the desired crystals containing both molecules. In contrast, the crystals consisting only of L-**3** was obtained when the combination of L-**3** and D-**1** was used.

As described earlier (Fig. 2 and S2–S4†), the crystal structure of L-**2** differs from the polymorphic crystals of L-**1**. Meanwhile, the quasiracemic crystal L-**2**/D-**1** (space group: $P2_1$) exhibits the same molecular arrangement as the racemic crystal DL-**1**, in which hydrophilic and hydrophobic regions are arranged alternately. Specifically, L-**1** in DL-**1** is replaced by L-**2** while maintaining the inversion symmetry of DL-**1** (Fig. 5a, S2–S4†, S12†, S13†, and Table S9†), although some quasiracemic crystals lack the inversion symmetry of the corresponding racemic crystal.[16] In the case of DL-**1**, a small void is present in front of the 7-position of the indole ring (Fig. S14). This structural feature likely allows the 7-position of one enantiomer to be substituted with a cyano group without altering the molecular packing. Another important point is that the cyano group does not participate in hydrogen bonding in L-**2**/D-**1**. In the

enantiomeric crystals of L-**2** and L-**3**, both the cyano and aza groups at the 7-position form hydrogen bonds in addition to those involving the amino acid moiety, resulting in different crystal structures compared with L-**1**. The preferential formation of enantiomeric crystals of L-**3** from the mixture of L-**3** and D-**1** should be attributed to the strong basicity of the aza moiety to form intermolecular hydrogen bonds. In contrast, L-**2** has a less basic cyano group, allowing it to preferentially arrange complementarily with D-**1** to form quasiracemic crystals (Fig. S15).

In L-**2**/D-**1**, a dimer is formed between L-**2** and D-**1** through an $R_2^2(10)$ motif involving the amino cation (N1–H1) and the oxygen atom (O1) of the carboxylate group (Fig. 5a: blue; Table S10 and S11†). Furthermore, two $C_1^1(5)$ hydrogen bonds (N1L–H2L···O1L and N1D–H2D ··· O1D, Fig. 5a: gray) are formed along the *a*-axis, and two additional $C_1^1(5)$ hydrogen bonds (N1L–H3L···O2L and N1D–H3D···O2D, Fig. S13b: green) are formed along the *b*-axis. These hydrogen bonding interactions give rise to the layered structure with alternating hydrophilic and hydrophobic regions extending in both directions.

The BFDH analysis revealed that crystal growth occurred along the *bc*-plane in the racemic crystal DL-**1** and along the *b*-axis in the quasiracemic crystal L-**2**/D-**1**. These results are consistent with experimental observations that the DL-**1** crystal formed plate-like morphology, while the L-**2**/D-**1** crystal exhibited needle-like morphology (Fig. 5b and S18†).

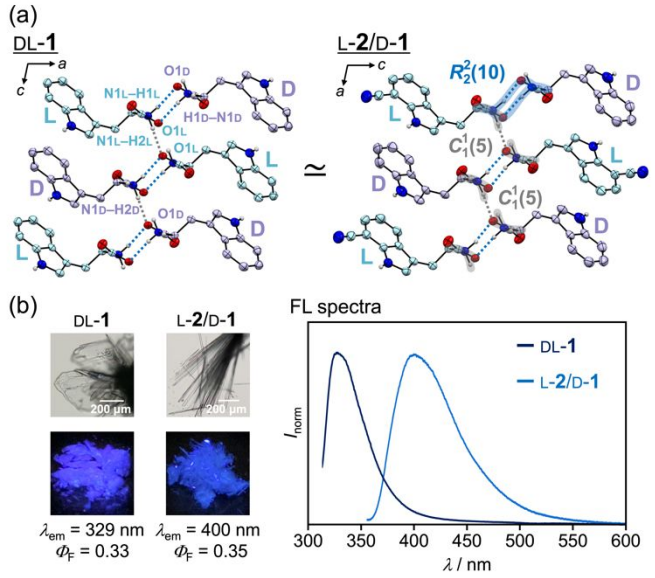

Fig. 5 (a) Crystal structures and (b) photographic images and fluorescence spectra of racemic crystal DL-**1** and quasiracemic crystal L-**2**/D-**1**.

Subsequently, we investigated the fluorescence properties of the racemic crystal DL-**1** and the quasiracemic crystal L-**2**/D-**1**. The racemic crystal DL-**1** exhibited blue-violet emission with a maximum emission wavelength (λ_{em}) of 329 nm and a fluorescence quantum yield (Φ_F) of 0.33. In contrast, the quasiracemic crystal L-**2**/D-**1** exhibited blue emission (λ_{em} = 400 nm, Φ_F = 0.35), originating from L-**2**, which was at a longer wavelength than that of the racemic crystal DL-**1** (Fig. 5b). Time-dependent density functional theory (TD-DFT) calculations of L-**2** and D-**1** at the CAM-B3LYP/6-31G(d) level of theory afforded theoretical fluorescence wavelengths of 337 nm and 285 nm, respectively (Fig. S19†). These results confirm that L-**2** exhibited fluorescence at a longer wavelength than D-**1**. The longer fluorescence wavelength of L-**2** can be attributed to the presence of the cyano group, which extends conjugation and stabilizes the LUMO energy level.

Conclusions

In summary, the crystal structures of 7-substituted tryptophan derivatives L-**2** and L-**3** were analyzed and compared with non-substituted **1**. The enantiomeric crystal of L-**2** exhibited a unique molecular arrangement distinct from that of L-**1**, characterized by hydrogen bonds involving the cyano and indole amino groups as well as the amino acid moiety. This arrangement resulted in fibrous crystal growth driven by continuous hydrogen bonds along the uniaxial direction. Meanwhile, L-**3** formed two types of crystals, *α* and *β*, due to intermolecular interactions through the nitrogen atom at the 7-position. Both *α*- and *β*-crystals formed uniaxially extending columnar structures. However, they adopted distinct molecular arrangements due to differences in the hydrogen-bonding roles of the oxygen atoms with adjacent columns. Notably, one-dimensional pores were confirmed in the *α*-crystal, which included solvent molecules. When L-**2** was co-crystallized with D-**1**, they formed the quasiracemic crystal L-**2**/D-**1**, which exhibited blue emission at a longer wavelength compared with the racemic crystal DL-**1**. These findings provide valuable insights into the design and development of amino acid derivative crystals as functional materials, highlighting their potential applications in fields such as molecular encapsulation and luminescent devices.

Experimental

General

^{1}H NMR spectra were recorded on a JEOL ECA-500 spectrometer using solvent residual signal [^{1}H NMR: D_2O (4.79 ppm)] as an internal standard. Fluorescence spectra were measured on a JASCO FP-8300 fluorescence spectrometer. The absolute fluorescence quantum yields were determined using a 100 mm *ϕ* integrating sphere JASCO ILF-835. The known compounds L-**2** and L-**3** were synthesized from L-serine with 7-cyanoindole and with 7-azaindole, respectively, using the engineered L-tryptophan synthase *β*-subunits as catalyst,[17] and their structures were unambiguously confirmed by single-crystal X-ray diffraction analysis. Other reagents and solvents were commercially available and were used as received.

Preparation of crystals

A 4.4×10^{-3} M aqueous solution (3.0 mL) of L-**2** (3.0 mg, 0.0131 mmol) was prepared, and vapor diffusion of acetonitrile into the aqueous solution (400 μL) of L-**2** afforded the fibrous crystals of L-**2**.

An aqueous solution (2.0 mL) of a 1:1 molar mixture of L-**2** (2.55 mg, 0.0125 mmol) and D-**1** (2.87 mg, 0.0125 mmol) was prepared, and vapor diffusion of ethanol into the aqueous solution (400 μL) of L-**2**/D-**1** afforded the needle-like quasiracemic crystals of L-**2**/D-**1**.

A 1.25×10^{-2} M aqueous solution (3.6 mL) of L-**3** (9.23 mg, 0.045 mmol) was prepared, and vapor diffusion of THF into the aqueous solution (400 μL) of L-**3** afforded the needle-like *α*-crystal of L-**3**. The elongated plate-like *β*-crystal of L-**3** was also prepared by vapor diffusion of acetonitrile into the aqueous solution (400 μL) of L-**3**.

Microcrystal electron diffraction analysis

The crystal structure of L-**2** was analyzed using the micro electron diffraction method (3D ED/MicroED). 3D ED/MicroED measurements were performed using the XtaLAB Synergy-ED (Rigaku Co., and JEOL Ltd.) equipped with CrysAlisPro for ED software and a HyPix-ED detector optimized for operation in the 3D ED/MicroED experimental setup.[18] The data sets were measured at room temperature (293 K) at a wavelength of 0.0251 Å corresponding to an acceleration voltage of 200 kV. The dose rate of the electron beam illuminating the crystals was set to ca. 0.01 $e^-/A^2/s$. The samples were loaded onto a carbon-film copper grid (TED PELLA INC., USA) by scooping up a slight amount of sample powder with a grid. The grid was set on a high tilt-type sample holder after excess sample was removed by tapping the tweezer holding the grid. All data collection steps, including searching for quality crystals, diffraction image acquisition, intensity extraction, and primary space group determination, were performed using a CrysAlisPro for ED instrument (Rigaku Corporation, Tokyo, Japan). During the test, all crystals were rotated continuously at 1~1.2°/s, and diffraction images were extracted every 0.15°. The tilt angle range for each crystal was −60° to 60° for a total of 120°. The initial phases were determined by a direct method using SHELXD,[19] and the obtained structure was refined by the full-matrix least-squares method using SHELXL[20] on the Olex2[21] single-crystal structure analysis platform. The structure was kinetically refined, and the dynamic effect was not considered.

X-ray crystallography

The crystalline samples were mounted on a microloop. All measurements were made on a Rigaku XtaLAB P200 diffractometer using multilayer mirror monochromated Cu–Kα radiation (λ = 1.54184 Å). The crystal-to-detector distance was 40.00 mm. Readout was performed in the 0.172 mm pixel mode. Data were collected and processed using CrysAlisPro (Rigaku Oxford Diffraction).[22] An empirical absorption correction was applied. The data were corrected for Lorentz and polarization effects. The structure of L-**3-β** was solved by direct methods (SHELXT Version 2014/4)[23] and expanded using Fourier techniques. The non-hydrogen atoms were refined anisotropically. Hydrogen atoms were refined using the riding model. All calculations of L-**3-β** were performed using the CrystalStructure[24] crystallographic software package except for refinement, which was performed using SHELXL Version 2014/7.[25] Using Olex2,[21] the structures of L-**2**, L-**3-α**, and L-**2**/D-**1** were solved with the SHELXT Version 2018/2[26] structure solution program using Intrinsic Phasing. The refinement was carried out with the SHELXL Version 2018/3[20] refinement package using least squares minimization.

Theoretical calculations

The theoretical calculations were performed using the Gaussian 16 program.[27] The molecular structures, obtained from the single-crystal X-ray diffraction analysis, were used as a starting point. Theoretical absorption and fluorescence wavelengths were calculated using TD-DFT calculations at the CAM-B3LYP/6-31G(d) level of theory.

Author contributions

All authors have approved the final version of this manuscript. CRediT author statement. YT: Data curation, Investigation, Validation, Visualization, Writing – original draft. MO: Methodology, Resources. TC: Methodology, Resources. SN: Funding acquisition, Methodology, Resources, Writing – review & editing. SI: Conceptualization, Funding acquisition, Investigation, Methodology, Project administration, Supervision, Validation, Writing – review & editing.

Conflicts of interest

There are no conflicts to declare.

Data availability

The data supporting this article have been included in the ESI.† Crystallographic data for L-**2**, L-**3-α**, L-**3-β**, and L-**2**/D-**1** have been deposited at the CCDC under deposition numbers 2419033 and 2419168–2419170 and can be obtained from https://www.ccdc.cam.ac.uk.

Acknowledgements

The authors are grateful to SPERA PHARMA, Inc. for the 3D ED/MicroED measurements of the crystal L-**2**. This work was partly supported by JST, PRESTO Grant Numbers JPMJPR20AB and JPMJPR21A3, Japan, and JSPS KAKENHI Grant Numbers JP24K01451 within the Grant-in-Aid for Scientific Research (B) and JP24K21781 within the Grant-in-Aid for Challenging Research (Pioneering).

Notes and references

1 H. Arifian, R. Maharani, S. Megantara, A. M. Gazzali and M. Muchtaridi, *Molecules*, 2022, **27**, 7631.
2 (*a*) C. H. Görbitz, K. W. Törnroos and G. M. Day, *Acta Cryst.*, 2012, **B68**, 549–557; (*b*) O. Al Rahal, C. E. Hughes, P. A. Wiliams, A. J. Logsdail, Y. Diskin-Posner and K. D. M. Harris, *Angew. Chem. Int. Ed.*, 2019, **58**, 18788–18792.
3 C. J. H. Smalley, H. E. Hoskyns, C. E. Hughes, D. N. Johnstone, T. Willhammar, M. T. Young, C. J. Pickard, A. J. Logsdail, P. A. Midgley and K. D. M. Harris, *Chem. Sci.*, 2022, **13**, 5277–5288.
4 (*a*) I. Azuri, E. Meirzadeh, D. Ehre, S. R. Cohen, A. M. Rappe, M. Lahav, I. Lubomirsky and L. Kronik, *Angew. Chem. Int. Ed.*, 2015, **54**, 13566–13570; (*b*) S. Guerin, S. A. M. Tofail and D. Thompson, *Cryst. Growth Des.*, 2018, **18**, 4844–4848; (*c*) D. Zaguri, S. Shaham-Niv, P. Chakraborty, Z. Arnon, P. Makam, S. Bera, S. Rencus-Lazar, P. R. Stoddart, E. Gazit and N. P. Reynolds, *ACS Appl. Mater. Interfaces*, 2020, **12**, 21992–22001; (*d*) X. Qiu, Y. Li, Y. hua, D. Liu, K. Zhou, Y. Wang and H. Guo, *Spectrochim. Acta, Part A*, 2022, **283**, 121719; (*e*) W. Ji, B. Xue, Z. A. Arnon, H. Yuan, S. Bera, Q. Li, D. Zaguri, N. P. Reynolds, H. Li, Y. Chen, S. Gilead, S. Rencus-Lazar, J. Li, R. Yang, Y. Cao and E. Gazit, *ACS Nano*, 2019, **13**, 14477–14485.

5 (*a*) M. Kitamura, *J. Cryst. Growth*, 2002, **237–239**, 2205–2214; (*b*) T. Shimizu, H. Yoshiura, H. Nagano and I. Hirasawa, *Chem. Eng. Technol.*, 2014, **37**, 1427–1430; (*c*) V. Yu. Torbeev, E. Shavit, I. Weissbuch, L. Leiserowitz and M. Lahav, *Cryst. Growth Des.*, 2005, **5**, 2190–2196; (*d*) J. Chen and B. L. Trout, *J. Phys. Chem. B*, 2010, **114**, 13764–13772.

6 (*a*) E. Mishuk, I. Weissbuch, M. Lahav and I. Lubomirsky, *Cryst. Growth Des.*, 2014, **14**, 3839–3848; (*b*) S. Guerin, J. O'Donnell, E. U. Haq, C. McKeown, C. Silien, F. M. F. Rhen, T. Soulimane, S. A. M. Tofail and D. Thompson, *Phys. Rev. Lett.*, 2019, **122**, 047701; (*c*) K. Ishizaki, D. Takagi, T. Asahi, M. Kuramochi and T. Taniguchi, *Cryst. Growth Des.*, 2023, **23**, 5330–5337.

7 (*a*) I. L. Karle and J. Karle, *J. Am. Chem. Soc.*, 1966, **88**, 24–27; (*b*) A. M. Lineberry, E. T. Benjamin, R. Davis, W. S. Kassel and K. A. Wheeler, *Cryst. Growth Des.*, 2008, **8**, 612–619; (*c*) M.E. Breen, S. L. Tameze, W. G. Dougherty, W. S. Kassel and K. A. Wheeler, *Cryst. Growth Des.*, 2008, **8**, 3863–3870.

8 (*a*) K. A. Wheeler, R. C. Grove, R. E. Davis and W. S. Kassel, *Angew. Chem. Int. Ed.*, 2008, **47**, 78–81; (*b*) J. T. A. Jones, T. Hasell, X. Wu, J. Bacsa, K. E. Jelfs, M. Schmidtmann, S. Y. Chong, D. J. Adams, A. Trewin, F. Schiffman, F. Cora, B. Slater, A. Steiner, G. M. Day and A. I. Cooper, *Nature*, 2011, **474**, 367–371; (*c*) S. Ito, K. Ono and N. Iwasawa, *J. Am. Chem. Soc.*, 2012, **134**, 13962–13965; (*d*) M. Kimoto, S. Sugiyama, K. Kumano, S. Inagaki and S. Ito, *J. Am. Chem. Soc.*, 2024, **146**, 17559–17565.

9 (*a*) A. I. Isakov, H. Lorenz, A. A. Zolotarev Jr and E. N. Kotelnikova, *CrystEngComm*, 2020, **22**, 986–997; (*b*) O. S. Tiwari, R. Aizen, M. Meli, G. Colombo, L. J. Shimon, N. Tal and E. Gazit, *ACS Nano*, 2023, **17**, 3506–3517.

10 (*a*) M. Sosa-Rivadeneyra, A. Zavala, J. F. Rivas-Silva, D. Uriza-Prias and S. Bernès, *Cryst. Growth Des.*, 2023, **23**, 7031–7036; (*b*) Y. Li, Y. Zhao and Y. Zhang, *Chirality*, 2015, **27**, 88–94.

11 (*a*) A. Wakahara, M. Kido, T. Fujiwara and K.-i. Tomita, *Bull. Chem. Soc. Jpn*., 1973, **46**, 2475–2480; (*b*) B. B. Ivanova and M. Spiteller, *Cryst. Growth Des*., 2010, **10**, 2470–2474.

12 M. C. Etter, J. C. MacDonald and J. Bernstein, *Acta Cryst.*, 1990, **B46**, 256–262.

13 J. Donnay and D. Harker, *Am. Mineral.* 1937, **22**, 446–467.

14 C. F. Macrae, P. R. Edgington, P. McCabe, E. Pidcock, G. P. Shields, R. Taylor, M. Towler and J. van de Streek, *J. Appl. Crystallogr.*, 2006, **39**, 453–457.

15 P. van der Sluis and A. L. Spek, *Acta Crystallogr*., *Sect. A*, 1990, **46**, 194–201.

16 B. Dalhus and C. H. Görbitz, *Acta Cryst.*, 1999, **C55**, 1547–1555.

17 H. Araseki, N. Sugishima, T. Chisuga and S. Nakano, *ChemBioChem*, 2024, **25**, e202400036.

18 S. Ito, F. J. White, E. Okunishi, Y. Aoyama, A. Yamano, H. Sato, J. D. Ferrara, M. Jasnowski and M. Meyer, *CrystEngComm*, 2021, **23**, 8622–8630.

19 I. Usón and G. M. Sheldrick, *Acta Crystallogr. D*, 2018, **74**, 106–116.

20 G. M. Sheldrick, *Acta Crystallogr C*, 2015, **71**, 3–8.

21 O. V. Dolomanov, L. J. Bourhis, R. J. Gildea, J. A. K. Howard and H. Puschmann, *J. Appl. Cryst*., 2009, **42**, 339–341.

22 *CrysAlisPro: Data Collection and Processing Software*; Rigaku Corporation: Tokyo 196-8666, Japan, 2015.

23 G. Sheldrick, *Acta Cryst.*, 2014, **A70**, C1437.

24 *CrystalStructure 4.2.5: Crystal Structure Analysis Package*; Rigaku Corporation: Tokyo 196-8666, Japan, 2000-2017.

25 G. M. Sheldrick, *Acta Crystallogr., Sect. A: Found. Adv*., 2008, **64**, 112–122.

26 G. M. Sheldrick, *Acta Crystallogr., Sect. A: Found. Adv*., 2015, **71**, 3–8.

27 M. J. Frisch, G. W. Trucks, H. B. Schlegel, G. E. Scuseria, M. A. Robb, J. R. Cheeseman, G. Scalmani, V. Barone, G. A. Petersson, H. Nakatsuji, X. Li, M. Caricato, A. V. Marenich, J. Bloino, B. G. Janesko, R. Gomperts, B. Mennucci, H. P. Hratchian, J. V. Ortiz, A. F. Izmaylov, J. L. Sonnenberg, D. Williams-Young, F. Ding, F. Lipparini, F. Egidi, J. Goings, B. Peng, A. Petrone, T. Henderson, D. Ranasinghe, V. G. Zakrzewski, J. Gao, N. Rega, G. Zheng, W. Liang, M. Hada, M. Ehara, K. Toyota, R. Fukuda, J. Hasegawa, M. Ishida, T. Nakajima, Y. Honda, O. Kitao, H. Nakai, T. Vreven, K. Throssell, J. A. Montgomery, Jr., J. E. Peralta, F. Ogliaro, M. J. Bearpark, J. J. Heyd, E. N. Brothers, K. N. Kudin, V. N. Staroverov, T. A. Keith, R. Kobayashi, J. Normand, K. Raghavachari, A. P. Rendell, J. C. Burant, S. S. Iyengar, J. Tomasi, M. Cossi, J. M. Millam, M. Klene, C. Adamo, R. Cammi, J. W. Ochterski, R. L. Martin, K. Morokuma, O. Farkas, J. B. Foresman and D. J. Fox, Gaussian 16, Revision A.03, Gaussian, Inc., Wallingford CT, 2016.

Data Availability Statement

The data supporting this article have been included in the ESI.† Crystallographic data for L-**2**, L-**3-α**, L-**3-β**, and L-**2**/D-**1** have been deposited at the CCDC under deposition numbers 2419033 and 2419168–2419170 and can be obtained from https://www.ccdc.cam.ac.uk.